A Comparison of the Theoretical and Measured Performance of the Herschel/SPIRE Imaging Fourier Transform Spectrometer

Locke D. Spencer*[a], David A. Naylor[a], Bruce M. Swinyard[b]

[a]University of Lethbridge, 4401 University Drive, Lethbridge, Alberta, T1K 3M4, Canada;
[b]Space Science and Technology Department, Rutherford Appleton Laboratory, Chilton, Didcot, Oxfordshire, OX11 0QX, UK.

ABSTRACT

The Spectral and Photometric Imaging Receiver (SPIRE) is one of three scientific instruments on ESA's Herschel Space Observatory. An imaging Fourier transform spectrometer (IFTS) provides the medium resolution spectroscopic capabilities of SPIRE. This paper compares the measured performance of the SPIRE IFTS, as determined from flight model instrument verification tests, with theoretical expectations. This analysis includes a discussion of the instrument line shape, signal-to-noise, resolution, field of view and spectrometer sensitivity.

Keywords: Herschel, SPIRE, Imaging Fourier transform spectroscopy, instrumental line shape, performance testing, Mach-Zehnder

1. INTRODUCTION

The Spectral and Photometric Imaging Receiver (SPIRE)[1] is one of three scientific instruments on ESA's Herschel Space Observatory.[2] An imaging Fourier transform spectrometer (IFTS) provides the medium resolution spectroscopic capabilities of SPIRE. This paper determines the resolution of the SPIRE IFTS from a careful analysis of the instrumental line shape (ILS), based on measurements obtained during instrument testing. Spectrometer resolution, signal-to-noise (S/N) ratio, field of view (FOV) and spectrometer sensitivity are also discussed. Other aspects of the current status of SPIRE are found elsewhere in these proceedings.[3–7]

The analysis presented here is based upon data obtained during flight model instrument verification tests, namely the first and second proto-flight model tests (PFM1 and PFM2 respectively), which were conducted in the spring and fall of 2005 at the Rutherford Appleton Laboratory (RAL) in the UK. Additional flight model testing is scheduled for the summer of 2006.

In Fourier transform spectroscopy, interferograms are recorded over a finite range of optical path difference (OPD) determined by the length of the FTS translation stage. Theoretically, and in the ideal case, an interferogram need only be measured from the position of zero path difference (ZPD) in one direction due to the symmetric nature of the instrument. In practice, however, a short double-sided portion of the interferogram is needed to account for any asymmetries. Typically, interferograms are measured in terms of both negative and positive OPD, with ZPD being the reference; however it is not necessary that both positive and negative maximum displacements be set equal. The single-sided (SS) portion of the interferogram ranges from ZPD to the point of maximum optical path difference, L_{SS} (positive OPD). The complementary region of the interferogram, i.e. that extending from ZPD to the other extreme, $-L_{DS}$ (negative OPD), is referred to as the double-sided (DS) region (see Figure 1). The DS portion is used to correct for asymmetries in the interferogram by a process known as phase correction which is discussed in detail elsewhere.[8,9]

In practice an interferogram is measured over a finite OPD, which is equivalent to the product of an infinitely long interferogram and the envelope function, $Env(z)$, shown in Figure 1. The envelope function over the interval $z \in [-L_{DS}, L_{SS}]$, is defined as:

$$Env(z) = \begin{cases} 1 & z \in [-L_{DS}, L_{SS}] \\ 0 & \text{elsewhere} \end{cases} . \quad (1)$$

*E-mail: locke.spencer@uleth.ca, Telephone: 1 403 329 2719, Fax:1 403 329 2057

The multiplication of an interferogram by $Env(z)$ (a rectangle function) is equivalent to a convolution in the spectral domain by a sinc function (i.e. $ILS(\sigma)$), which produces the ILS given below. This is illustrated using an interferogram with an envelope ranging from $-L$ to L as follows:

$$ILS(\sigma) = \int_{-\infty}^{+\infty} Env(z) e^{-2\pi\sigma z} dz = 2L sinc(2\pi\sigma L). \quad (2)$$

From Equation 2 it can be shown that the full width at half maximum (FWHM) of the ILS is given by

$$ILS_{\rm FWHM} = \frac{1.207}{2L} \quad cm^{-1}, \quad (3)$$

demonstrating that the spectral resolution is inversely proportional to the maximum OPD. The right graph in Figure 1 illustrates the spectral ILS resulting from both the DS (L = 1.4 cm, $ILS_{\rm FWHM}$ = 0.431 cm^{-1}) and SS (L = 14 cm, $ILS_{\rm FWHM}$ = 0.0431 cm^{-1}) portions of the interferogram. Since unresolved spectral features measured with an FTS will reproduce the ILS, the ILS is most easily probed by observing an unresolved spectral feature. This paper investigates the ILS of the SPIRE IFTS as determined by measurements of unresolved spectral line sources, and compares the results with theory (Equations 2 & 3).

Another practical consideration in spectral analysis is optical divergence within the interferometer. For oblique rays transiting the interferometer, the effective off-axis OPD is less than that for the axial ray by a factor of $\cos(\beta)$, where β is the angle of the ray from the optical axis of the interferometer with respect to the pupil. Thus, the frequency of a monochromatic source on a non-central detector will occur at

$$\sigma = \sigma_o(1 - \cos(\beta)) \quad cm^{-1}. \quad (4)$$

Divergence within an FTS gives rise to the Jacquinot criterion[10] where the product of the spectrometer resolving power and divergent solid angle are related by $R\Omega = 2\pi$. This phenomenon is known as natural apodization and results in the interferogram being multiplied by a *sinc* function; or equivalently the spectrum being convolved with a rectangle function given by[11]

$$Rect(\sigma_r) = \int_{-\infty}^{+\infty} sinc(\frac{\sigma_o \Omega z}{2}) e^{-2\pi\sigma z} dz = (\frac{\pi}{\sigma_o \Omega}) Rect(\frac{\sigma_o \Omega}{2\pi}). \quad (5)$$

where σ_o is the frequency of the monochromatic source and Ω is the divergence within the interferometer. Thus a monochromatic source of frequency σ_o will be observed to be centered at $\sigma_o[1 - \frac{\Omega}{4\pi}]$ with a width of $\frac{\sigma_o \Omega}{2\pi}$.

This paper uses the spectral broadening and shift discussed above to investigate the angular separation of the SPIRE spectrometer detectors based upon measurements of unresolved spectral line sources obtained during the PFM1 and PFM2 instrument test campaigns.

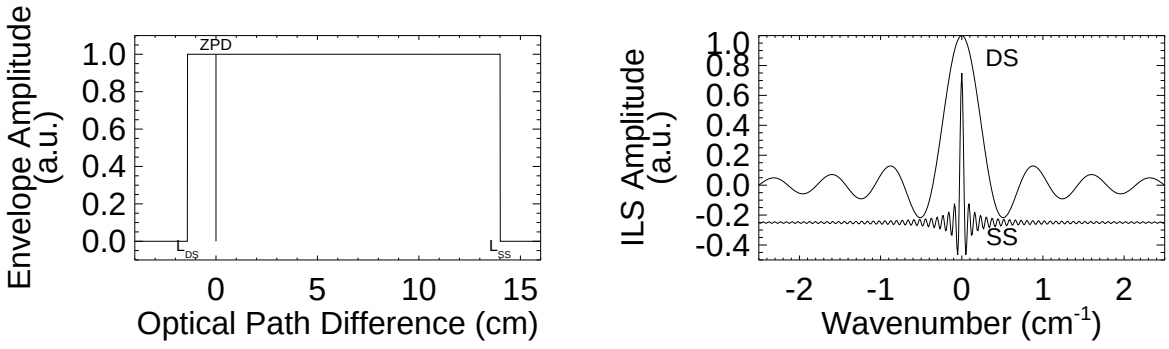

Figure 1. The finite optical path length of the IFTS translation stage available to SPIRE (left) and the resultant ILS of the SPIRE spectrometer (right). The DS and SS spectral ILSs differ in width by a factor of ten due to the ratio of the interferogram envelope widths (i.e. L_{DS} = 0.35 cm and L_{SS} = 3.5 cm for SPIRE). The SS ILS is offset vertically for clarity.

2. SPECTRAL LINE SOURCES

This paper discusses data taken in the PFM1 and PFM2 test campaigns involving the SPIRE IFTS. Although a myriad of tests were performed with the SPIRE instrument during these test campaigns, only those tests related to the ILS of the SPIRE spectrometer will be discussed here. Information regarding the test campaigns, in general, and other aspects of the SPIRE instrument are found elsewhere.[4–7] While the test campaigns lasted approximately one month each, the time assigned to measurements involving the spectrometer ILS was ∼5 hours for PFM1 and less than 1 hour for PFM2.

As discussed in section 1, the simplest way to determine the ILS of an FTS is to use an unresolved spectral line source. The unresolved spectral line sources used in the PFM1 and PFM2 test campaigns were a molecular laser and a photonic mixer,[12,13] respectively. Both of these sources are described below.

One of the SPIRE test facility subsystems is a molecular laser (Edinburgh Instruments model 295 FIR). In operation, the laser is optically pumped by a CO_2 laser, which is tuned to match the pumping transition of the molecular gas in the resonant cavity. A beamsplitter placed in the output path of the molecular laser directs a portion of the beam towards a pyroelectric detector, which monitors the laser output power. With the selection of CO_2 pump lines, variable cavity length, and selection of molecular gases, the resonant cavity is capable of providing a wide variety of laser lines throughout the far-infrared. Table 1 lists the pump states and transition lines used during PFM1 testing of the SPIRE spectrometer for either methanol (CH_3OH) or formic acid (HCOOH). Each of these transitions have been well studied and the corresponding frequencies are documented in the literature.[14]

A photonic mixer provided an alternative spectral line source for SPIRE instrument testing. The photonic mixer is part of a technology development effort by the Millimetre-Wave group of the Space Science Technology Department (SSTD) at RAL. The photonic mixer used during PFM2 testing accepts two compact near-infrared lasers operating at a wavelength of ∼1.55 μm (standard in the telecom industry) as input via a polarization maintaining fibre. The photonic mixer is controlled/tuned via a bias voltage and the temperature stabilized input lasers are tuned by voltage. The laser inputs are tuned to chosen wavelengths spectrally separated by several hundred gigahertz (GHz). The nonlinear effect of the photonic mixer generates coherent radiation at the difference frequency between the source lasers. At several hundred gigahertz, this difference is in the sub-millimetre spectral domain. The photonic mixer output is directed towards SPIRE via a radiating feedhorn and free space optics.

3. DATA ANALYSIS

Interferograms of the unresolved spectral sources directed towards individual pixels within both the spectrometer long-wavelength (SLW) and the spectrometer short-wavelength (SSW) arrays were recorded. The detectors within each array are organized in a hexagonal configuration with alpha-numeric names as indicated in Figure 2. While the spectrometer views the line sources, it is also subject to ambient radiation from the test laboratory environment. Thus the interferograms measured contain both interference fringes from the unresolved line, which are observed as sinusoidal oscillations throughout the length of the interferogram, and the broadband contribution from the background, which provides a large modulated signal component near ZPD. An example of this is shown in Figure 3.

Standard FTS processing routines were used in the reduction of the data to generate spectra; this included phase correction using the Forman method[8] to remove interferogram asymmetries, and multiple scan averaging to reduce noise. A least squares fitting routine is used to determine the amplitude, width, and central frequency of the sinc ILS for each spectral line. The uncertainty in the spectral line is related to the ILS width ($\mathrm{ILS_{FWHM}}$) and S/N by:[15]

$$\delta\sigma_o \propto \frac{\mathrm{ILS_{FWHM}}}{\mathrm{S/N}} \quad cm^{-1}. \tag{6}$$

A fit was also performed to the sinusoidal portion of the interferograms of the PFM1 data. The measured PFM1 frequencies are compared to their theoretical values. A similar analysis was performed on the PFM2 spectra, however, in this case the precise source frequencies, being difference frequencies, are unknown.

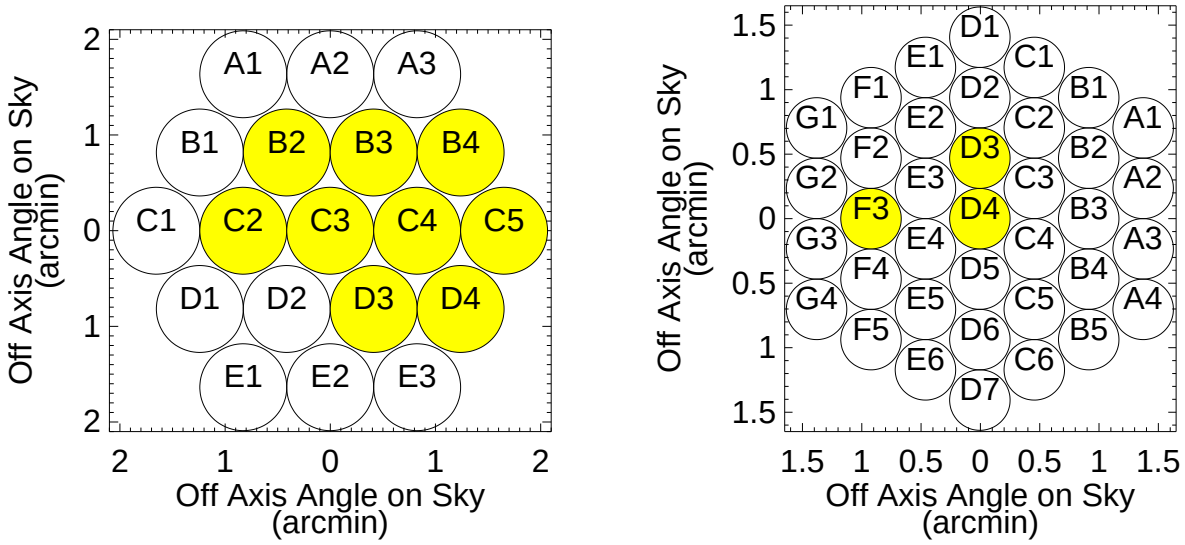

Figure 2. SLW (left) and SSW (right) array maps demonstrating detector orientation and off-axis angular separation with respect to the sky. Pixels tested during either of PFM1 or PFM2 are shaded.

3.1. Laser Lines

The PFM1 tests included the first spectral line data obtained with SPIRE. Table 1 summarizes the laser lines used during these tests. Six different pixels within both the SLW and SSW arrays were illuminated. The interferogram, shown in Figure 3, contains contributions from both the molecular laser and the room background. Unfortunately, during these measurements, the ambient radiation from the test laboratory environment causes the observed interferogram saturation near ZPD, which results in calibration and phase errors in the resulting spectrum. This figure also illustrates the sinusoidal oscillations within the interferogram produced by the laser. Figure 4 shows the spectrum generated using the data from Figure 3.

Table 1. Summary of FTS laser spectra taken during the PFM1 test campaign.

Date	Array/Pixel	N scans	Scan length (cm)	Gas	CO_2 Pump line	laser line (cm^{-1})
March 9	SLW C3	30	1.3/12.5	HCOOH	9R 20	23.1124893(7) 23.1143706(8)
March 9	SLW B2	23	1.3/12.5	HCOOH	9R 20	23.1124893(7) 23.1143706(8)
April 6	SSW D3	23	12.5	CH_3OH	9R 10	42.9296823(7)
April 7	SLW C2	10	12.5	HCOOH	9R 4	33.0821464(5)
April 7	SSW F3	10	12.5	HCOOH	9R 4	33.0821464(5)
April 7	SLW C3	6	12.5	HCOOH	9R 4	33.0821464(5)
April 7	SSW D4	6	12.5	HCOOH	9R 4	33.0821464(5)
April 8	SLW C2	3	12.5	HCOOH	9R 28	19.4925817(6) 19.4930921(2)
April 8	SLW C3	3	12.5	HCOOH	9R 28	19.4925817(6) 19.4930921(2)

Table 2 shows the retrieved line centres and uncertainties (in parentheses) from least squares fitting of both the spectra and interferograms. The line centres are compared to both the theoretical line centres as well as the spectral resolution of the scan. All of the line centers are within one spectral resolution element, with the exception of the scans involving pixels SLW C2 and SSW F3 observing the 33.082 cm^{-1} line. In this case

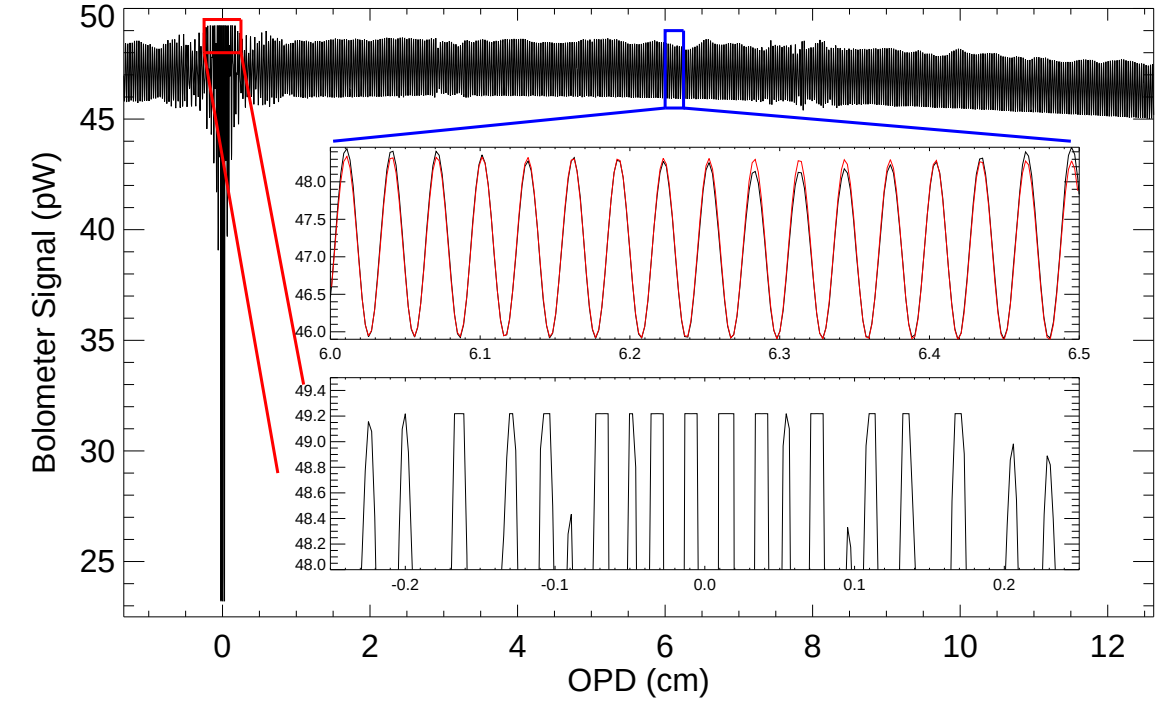

Figure 3. Sample interferogram from PFM1 FTS scans using the molecular laser. The upper inset within the plot shows the sinusoidal signal due to the laser source (with a fit to the sinusoid also shown). The lower inset illustrates detector saturation near ZPD.

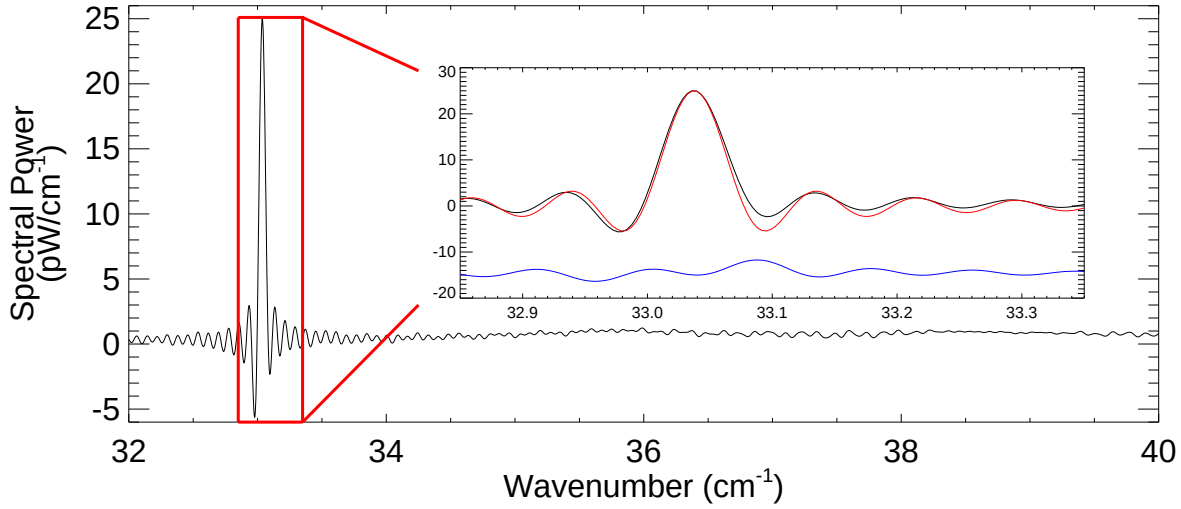

Figure 4. The spectrum resulting from the interferogram shown in Figure 3. The inset shows a close up view near the line centre as well as the difference between the line and the sinc fit (vertically offset for clarity).

examination of this data reveals a discontinuity in the spectral phase within close proximity to the spectral line. Although the line centre is shifted, the ILS is still observed to follow the expected sinc profile. All of the ILS widths measured were consistent with theory. Discussion of the spectral and interferogram S/N values is presented in section 4.1.

Table 2. PFM1 Spectrum/Interferogram fit summary.

	Spectrum				Interferogram			
Array/ Pixel	σ_{Spectrum} (cm^{-1})	$\frac{\sigma_o - \sigma}{\sigma_o}$ (%)	$\frac{\sigma_o - \sigma}{\Delta\sigma}$ (%)	S/N	$\sigma_{\text{Interferogram}}$ (cm^{-1})	$\frac{\sigma_o - \sigma}{\sigma_o}$ (%)	$\frac{\sigma_o - \sigma}{\Delta\sigma}$ (%)	S/N
SLW C2	19.46(8)	0.13(0)	6(3)	40	19.46(7)	0.1(3)	6(6)	9
SLW C3	19.47(9)	0.07(3)	3(5)	33	19.47(8)	0.0(8)	3(8)	33
SLW B2	23.08(9)	0.10(6)	6.(3)	16	23.0(9)	0.(1)	(7)	16
SLW C3	23.09(9)	0.06(4)	3.(9)	12	23.0(9)	0.(1)	(7)	11
SLW C2	33.03(7)	0.13(6)	11(3)	24	33.0(3)	0.1(4)	1(19)	37
SLW C3	33.05(9)	0.06(9)	5(7)	35	33.05(8)	0.0(7)	6(2)	19
SSW F3	33.03(8)	0.13(5)	11(1)	29	33.0(3)	0.1(4)	1(17)	26
SSW D4	33.05(9)	0.07(1)	5(9)	40	33.05(8)	0.0(7)	6(1)	21
SSW D3	42.89(6)	0.07(9)	8(5)	22	42.89(2)	0.0(9)	9(3)	4

3.2. Photomixer Lines

The PFM2 test campaign included scans using an unresolved source from the photonic mixer. Seven interferograms were obtained with the photonic mixer, each measured out to 12.5 cm OPD, and illuminating SLW pixel C4 of the SPIRE IFTS (see Figure 2). For three of these scans the photonic mixer was tuned to produce a spectral line at ∼509.5 GHz; for the other scans the mixer was tuned to ∼601 GHz. In both cases the dominant contribution to the spectrum was the ambient broadband background radiation in the laboratory. However, since both observations were taken under similar conditions (i.e. source position, optics, detector configuration, laboratory atmospheric opacity, etc.) and were closely spaced in time, it is reasonable to expect that the contribution from the background radiation will be constant (see Figure 5). Thus by differencing the spectra from the two line sources the dominant background continuum will be removed, isolating the spectral line information. The resulting difference spectra is fitted with two sinc ILS, one of which is expected to appear inverted due to the differencing involved. Also visible in Figure 5 are channel fringes which are discussed in section 4.2. General details on other aspects of the PFM2 test campaign may be found elsewhere.[4–7]

The photonic mixer is a tunable device, and thus the precise emission frequency is unknown, however, this knowledge is unnecessary in its use in determining the ILS since it is the line profile, not the line centre, that is important. Although the photonic mixer illuminated pixel SLW C4, some energy is detected by neighboring pixels (SLW B3, B4, C5, D3, and D4), albeit at significantly reduced amounts. Serendipitously, this allows for a study of the variation of the line center with respect to the spectrometer optical axis (see section 4.3). Although the S/N is not sufficiently large on the neighboring pixels to obtain a reliable fit of both the line centre and width, a reasonable measure of the line center may be obtained. Figure 6 shows both the spectra (left) and spectral difference (right), i.e. the two sinc features, for pixels SLW B3 and C4. The lines are not directly visible within the spectrum of B3 until the differencing technique is employed. Although spectra from only two pixels are shown, the remaining pixels (B4, C3, D3, and D4) show similar structure, that is, lines appropriately centered with varying amplitudes depending on the pixel orientation to the source. Analysis of the line centers observed, after accounting for the off-axis frequency shift, yields photomixer line frequencies of 17.00 ± 0.01 cm^{-1} and 20.07 ± 0.01 cm^{-1} (i.e. 509.7 ± 0.3 GHz and 601.7 ± 0.4 GHz, respectively). The line centres are in agreement with the expected values and both uncertainties are less than a spectral resolution element. Section 4.3 discusses the angular orientation of the illuminated detectors and section 4.4 discusses the spectrometer sensitivity, determined from these measurements.

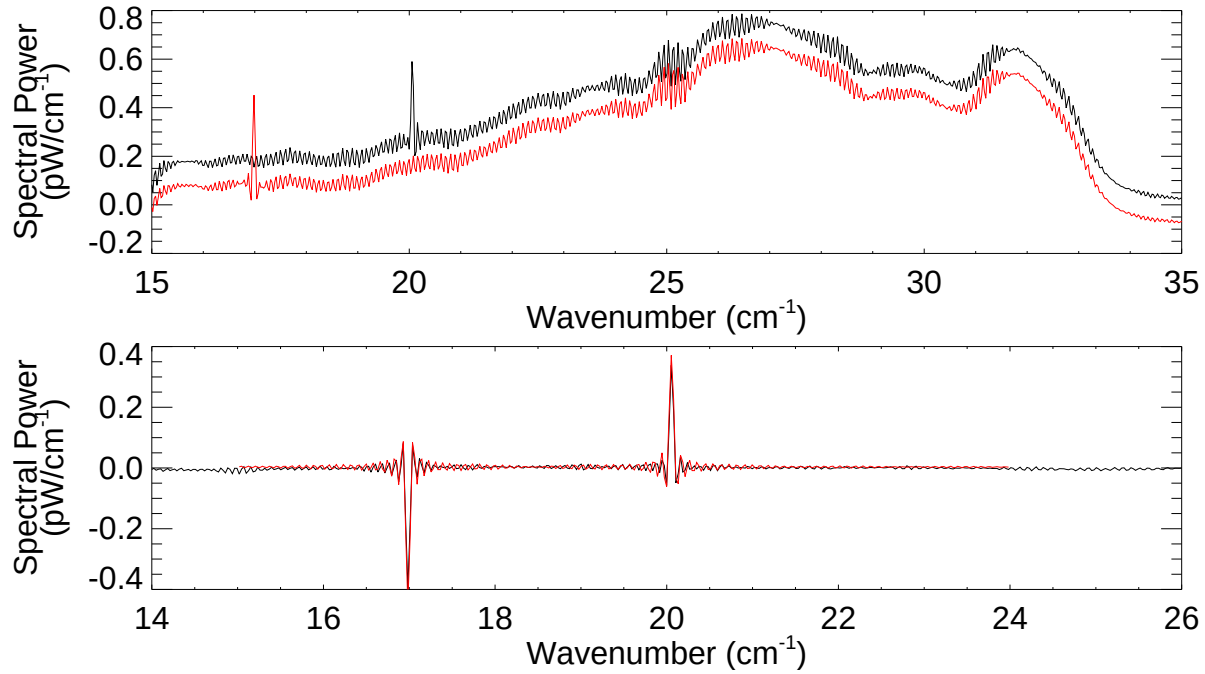

Figure 5. Measured spectra and difference for both photonic mixer frequencies. A fit of the ILS to the difference is also shown.

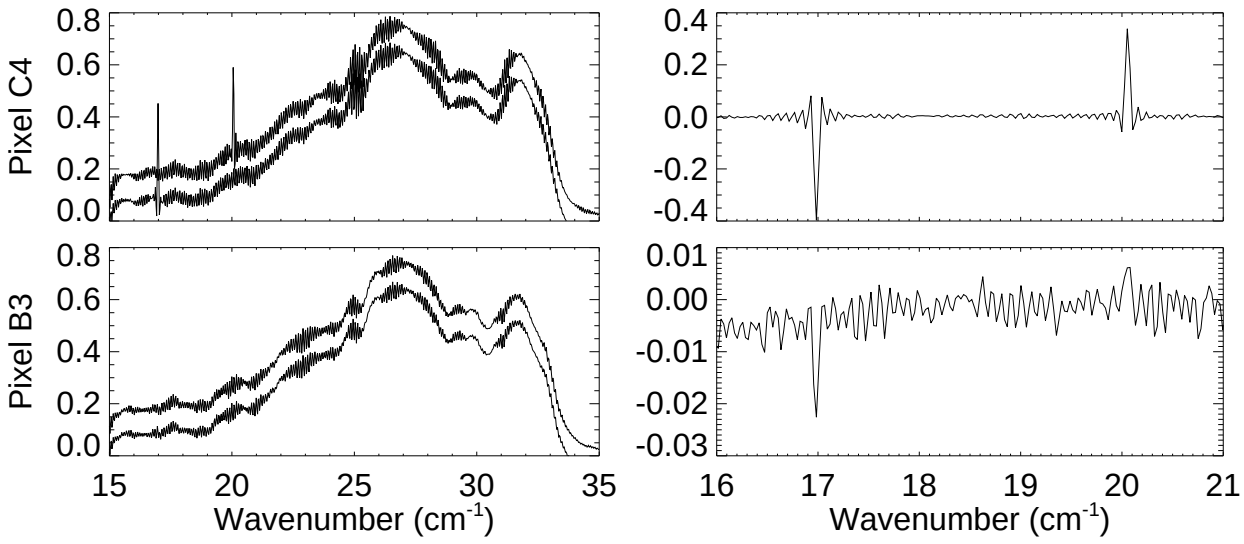

Figure 6. PFM2 photonic mixer spectra for two neighboring pixels (SLW B3 and C4). The left hand column shows the spectra for each of the two lines (offset for clarity). The right hand column shows the corresponding spectral difference.

4. DISCUSSION

4.1. Signal-to-Noise

Signal-to-noise estimates were taken throughout this analysis by comparing root-mean-square residuals of the noise after subtraction of the fit (and background if applicable). Interferograms were fitted with a sinusoid to represent the line source in the interference pattern, while spectra were each fitted with a sinc function and a rectangular convolution, to account for the instrument ILS and natural apodization, respectively (see equation 5). The S/N ratio is also important in determining the detector line sensitivity presented in section 4.4. The S/N in the interferogram and spectrum are related through Perseval's theorem.[16]

Although a comparison of the fitting of the line frequency in the spectrum and the sinusoid frequency in the interferogram may appear redundant, especially in the case of the molecular laser where the exact source frequency is known, comparing measurements in both Fourier domains is non-trivial. Since natural apodization is equivalent to multiplication of the interferogram by a sinc envelope (equation 5), the effective frequency observed throughout the interferogram will vary. A frequency of a sinusoid fit to the interferogram will thus vary depending on the region of the interferogram selected for study. Moreover, variations in the source intensity within an observation will be problematic as they are indistinguishable from apodization affects. This will influence the observed sinusoidal frequency throughout the interferogram and thus the line position and shape in the spectrum.

Another example of differences of the derived interferogram and spectral S/N is phase error. For example, a phase error in an interferogram has no effect on fitting a sinusoid to the data but has serious implications for the spectral fit if left uncorrected.

S/N reduction may also be caused by uncharacterized spectral background. The spectral differencing employed in the PFM2 data analysis greatly improved the S/N of the line source spectra by removal of the background continuum. This is observed in figure 5.

When an account is taken of the above effects, the S/N in the spectrum and interferogram are in general agreement. The corresponding S/N values for the PFM1 tests are shown in table 2.

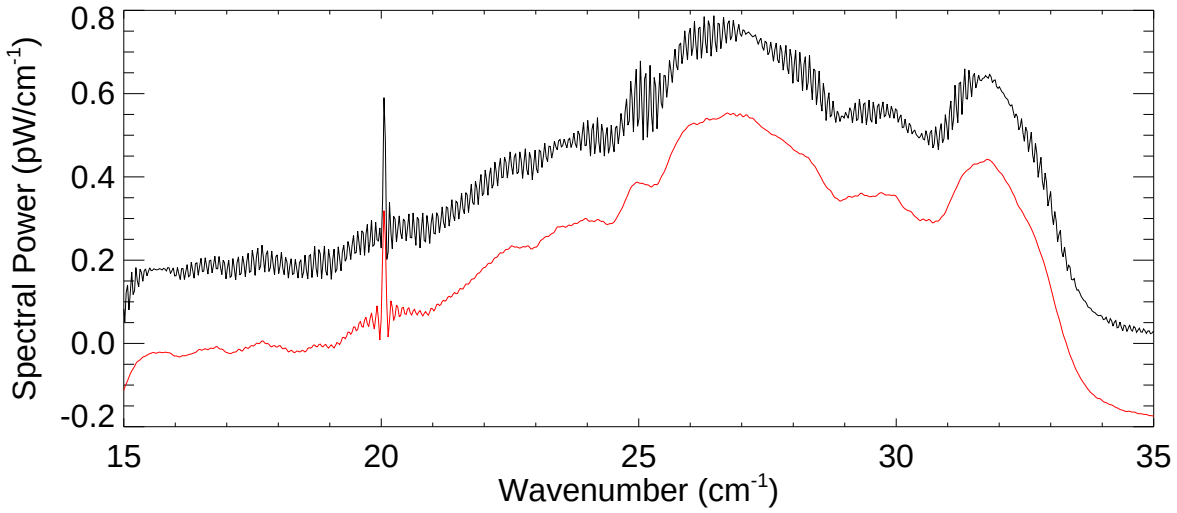

Figure 7. High and low resolution spectra from PFM2 photonic mixer data illustrating the presence of spectrometer channel fringing. The lower curve is from an interferogram taken out to 10 cm OPD and the upper spectrum is from the full resolution interferogram including the channel fringe region.

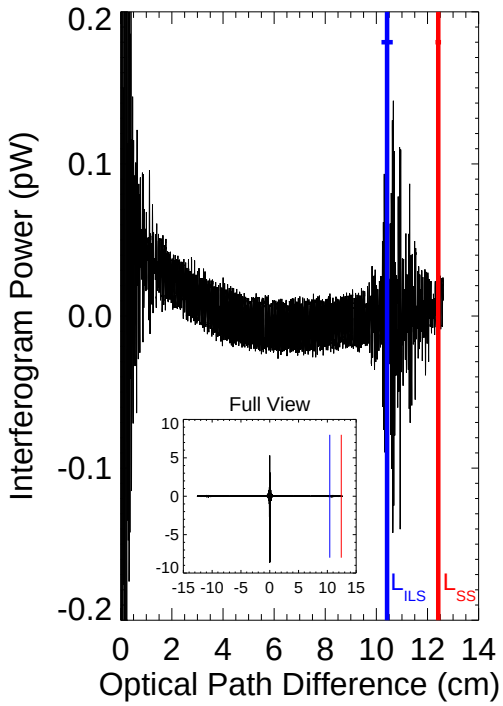

Figure 8. A PFM2 interferogram with channel fringes. Vertical bars indicate L_{ILS} and L_{SS}, errors are shown using a horizontal bar near the top.

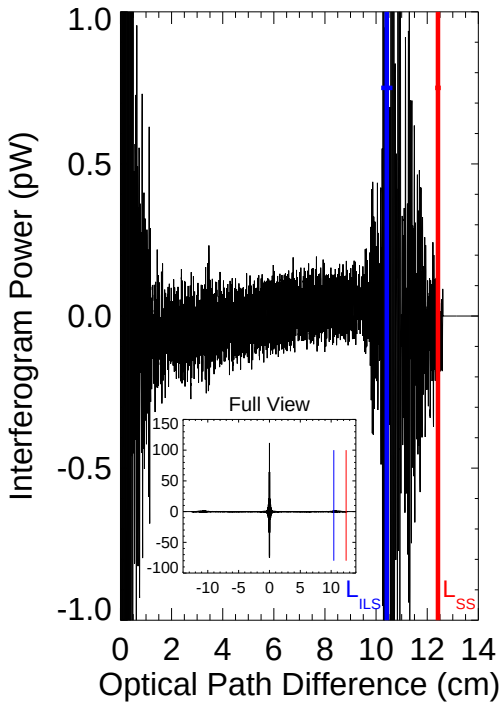

Figure 9. A PFM1 interferogram with observed channel fringes. L_{ILS} and L_{SS} from PFM2 are shown for comparison.

4.2. Spectrometer Channel Fringes

Figure 5 shows an unresolved spectral feature superimposed upon a broad background. The background appears to have a high frequency component which results from channel fringes within the spectrometer.[7] Figure 7 shows spectra from the same interferogram taken at different resolutions. The upper curve shows the spectrum resulting from the full scan length of the interferogram. The lower curve shows the resultant spectrum with the interferogram truncated at 10 cm OPD. The structure of the background continuum is similar; however, the channel fringes are significantly reduced in amplitude. Since the width of the ILS is related to the interferogram OPD (equation 2), a fit of the ILS derived from the full resolution spectrum should reveal the interferogram scan length. This, however, was not the case. A fit of the ILS for each of the interferograms yielded an L_{SS} of 10.4 ± 0.2 cm where the actual interferograms were measured out to 12.4 ± 0.1 cm. Upon inspection of the interferograms in question (see Figure 8), it is observed that the OPD region encompassed by this difference, i.e. [L_{ILS} , L_{SS}], has a clearly identified channel fringe. Although the interferogram is recorded out to ~12.42 cm OPD, the signal beyond ~10.42 cm OPD does not result in increased spectral resolution.

Interferogram channel fringes were not typically observed in PFM1 measurements using the molecular laser. This is because the intensity of the molecular laser dominates the modulation within the interferogram due to the channel fringe; and thus the channel fringes, which are most readily observed under a broad rather than narrow spectral source, are not evident. An example of the PFM1 channel fringe is shown in Figure 9.

Analysis has been performed[7] demonstrating that resonant optical cavities can result between the field lenses (at the entrance to the detector assemblies) and the front and back of the detector assemblies. It is anticipated that new field lenses, which have an anti-reflection coating, will reduce the channel fringes by as much as a factor of two; their performance will be evaluated in future test campaigns. Further details on the SPIRE spectrometer

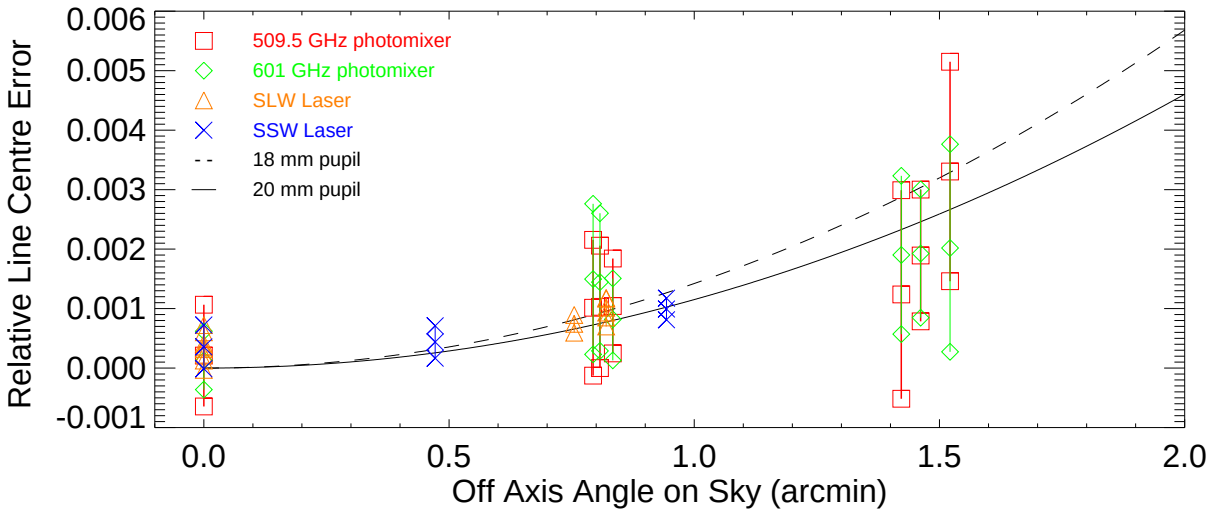

Figure 10. A comparison of the line centre deviation across the telescope sky. The dashed line is the expected angular position for an 18 mm FTS entrance pupil and the solid line is for a 20 mm FTS entrance pupil.

channel fringes are discussed elsewhere in these proceedings.[7]

4.3. Off-Axis Calculations

Angular separation of a detector from the optical axis with respect to the FTS pupil, β, is related to the angle of the detector on the sky, α, as follows

$$\alpha = \frac{D_{\rm pupil}}{D_{\rm Telescope}}\beta, \tag{7}$$

where the D's represent the respective pupil diameters. For the SPIRE spectrometer, the FTS pupil diameter is 18-20 mm, with the entrance pupil being 3.3m, namely that due to the Herschel Primary mirror. The expected frequency shift for off-axis detectors is given in equation 4. Figure 10 shows the axial variation of both the molecular laser and photomixer line centres plotted against the angular position on the sky. This figure also shows the expected frequency shift as a function of off-axis angle for two pupil sizes within the FTS. While the experimental data show significant scatter this in not inconsistent with theory.

4.4. Detector Sensitivity

Based on the lines detected via differencing of the spectra obtained with the photonic mixer, an estimate of the SPIRE spectrometer line sensitivity is possible. For the frequency region in question, the line sensitivity quoted in the SPIRE Sensitivity Model (SPIRE-QMW-NOT-000642)[17,18] is estimated to be $7.1 - 9.9 \times 10^{-17}$ ($\Delta F(5\sigma; 1-hr)$) Wm^{-2}. The 5-σ; 1-hr line sensitivity, ΔF, is determined as follows

$$\Delta F = \frac{I\Delta\sigma}{\pi(r)^2\eta} \quad W\ m^{-2}(5-\sigma; 1-\text{hour}). \tag{8}$$

where I is the line strength (W/cm^{-1}), $\Delta\sigma$ is the spectral resolution (cm^{-1}), r is the telescope primary mirror radius (m), η is the telescope obscuration factor (87% for Herschel), and additional multiplicative factors were also included to normalize the data to 5-σ S/N and 1 hour scan times. Using the above formula, the sensitivity was calculated using all of the available PFM2 spectral line measurements; these data are presented in table 3. The spectral line sensitivity was determined to be $7.2 \pm 0.1 \times 10^{-17} W\ m^{-2}$ ($\Delta F(5\sigma; 1-hr)$) from the SLW C4 measurements. The sensitivities derived from the other pixels are in close agreement with this value, however, their lower S/N results in greater uncertainty. It is encouraging that there is such close agreement between the derived sensitivities and those determined through theoretical modeling.

Table 3. SPIRE spectrometer line sensitivity determination.

Pixel	low frequency line			high frequency line		
	Power (fW/cm^{-1})	S/N	Δ F (10^{-17} W m^{-2})	Power (fW/cm^{-1})	S/N	Δ F (10^{-17} W m^{-2})
SLW B3	14 ± 5	3	6 ± 2	20 ± 9	2	11 ± 5
SLW B4	61 ± 5	11	6.5 ± 0.6	82 ± 6	14	6.6 ± 0.5
SLW C3	18 ± 9	2	10 ± 5	9 ± 5	2	6 ± 3
SLW C4	398 ± 6	63	7.2 ± 0.1	341 ± 6	54	7.2 ± 0.1
SLW C5	23 ± 6	4	6 ± 2	20 ± 4	5	5 ± 1
SLW D3	20 ± 6	3	7 ± 2	7 ± 3	2	4 ± 2
SLW D4	6 ± 4	1	5 ± 3	28 ± 8	3	10 ± 3

5. CONCLUSIONS

The ILS of the SPIRE spectrometer has been measured from observations of unresolved far-IR sources. The results are in excellent agreement with theory. The effects on the observed spectral frequency as a function of angular position of the detector on the sky, while well below the resolution of the spectrometer, are consistent with the theoretical model. Finally, the SPIRE spectrometer line sensitivity, as determined from this analysis, is found to be in close agreement with that predicted from theoretical modeling. Moreover, the analysis presented here will play an important role in planning the measurements that will be obtained in future instrument test campaigns.

6. ACKNOWLEDGEMENTS

The authors wish to thank Marc Ferlet for his assistance with the calibration sources and far-IR optics; Edward Polehampton and Tanya Lim for their assistance in the testing and data analysis; Steve Guest for his valuable assistance with the database and Java; Asier Aramburu and Sunil Sidher for their assistance with the SPIRE database, as well as all of the long hours in the control room; Matt Griffin et. al. in Cardiff for useful feedback during the SDAG meetings and otherwise; Peter Davis, Ken King, and Dave Smith for their managerial assistance; Trevor Fulton for his data processing expertise; Tanya Lim and Sarah Leeks for their dedication to instrument testing; Alan Pearce and Mike Trower for their technical assistance; John Lindner for his editorial expertise; as well as the countless others who form the SPIRE group within the SSTD at RAL, and the SPIRE consortium in general. This research has been funded by the CSA, NSERC, PPARC, CIPI, and CFI.

REFERENCES

1. M. Griffin, B. Swinyard, and L. Vigroux, "The spire instrument for first," in *UV, Optical and IR Space Telescopes and Instruments*, J. B. Breckinridge and P. Jakobsen, eds., **4013**, pp. 142–151, Proceedings of the International Society for Optical Engineering, 2000.
2. G. L. Pilbratt, "Herschel mission: Status and observing opportunities," in *Optical, Infrared, and Millimeter Space Telescopes*, J. C. Mather, ed., **5487**, pp. 401–412, Proceedings of the International Society for Optical Engineering, 2004.
3. G. L. Pilbratt, "Herschel mission: status and observing opportunities," in *Space Telescopes and Instrumentation I: Optical, Infrared, and Millimeter (this volume)*, **6265**, Proceedings of the International Society for Optical Engineering, 2006.
4. M. J. Griffin and B. M. Swinyard, "Herschel-spire: design, performance, and scientific capabilities," in *Space Telescopes and Instrumentation I: Optical, Infrared, and Millimeter (this volume)*, **6265**, Proceedings of the International Society for Optical Engineering, 2006.
5. B. M. Swinyard, K. Dohlen, M. Ferlet, J. Glenn, and J. J. Bock, "Optical performance characterization of herschel/spire," in *Space Telescopes and Instrumentation I: Optical, Infrared, and Millimeter (this volume)*, **6265**, Proceedings of the International Society for Optical Engineering, 2006.

6. T. L. Lim, B. M. Swinyard, A. A. Aramburu, J. J. Bock, M. J. Ferlet, and T. R. Fulton, "Preliminary results from herschel-spire flight model testing," in *Space Telescopes and Instrumentation I: Optical, Infrared, and Millimeter (this volume)*, **6265**, Proceedings of the International Society for Optical Engineering, 2006.
7. D. A. Naylor, J.-P. Baluteau, P. Davis-Imhof, M. J. Ferlet, T. R. Fulton, and B. M. Swinyard, "Performance evaluation of the herschel/spire imaging fourier transform spectrometer," in *Space Telescopes and Instrumentation I: Optical, Infrared, and Millimeter (this volume)*, **6265**, Proceedings of the International Society for Optical Engineering, 2006.
8. L. D. Spencer, "Spectral characterization of the herschel spire photometer," Master's thesis, University of Lethbridge, Lethbridge, AB, 2005.
9. L. D. Spencer and D. A. Naylor, "Optimization of FTS Phase Correction Parameters," in *Fourier transform spectroscopy topical meeting*, Optical Society of America, Feb 2005.
10. P. Jacquinot, "New developements in interference spectroscopy," *Rep. Prog. Phys.* **23**, pp. 267–312, 1960.
11. R. J. Bell, *Introductory Fourier Transform Spectroscopy*, Academic Press, New York, 1972.
12. P. Huggard, B. Ellison, P. Shen, N. Gomes, P. Davies, W. Shullue, A. Vaccari, and J. Payne, "Efficient Generation of Guided Millimeter-Wave Power by Photomixing," *IEEE Photonics Technology Letters* **14**, pp. 197 – 199, Feb. 2002.
13. P. Huggard, B. Ellison, P. Shen, N. Gomes, P. Davies, W. Shullue, A. Vaccari, and J. Payne, "Generation of Millimetre and Sub-millimetre Waves by Photomixing in 1.55 μm Wavelength Photodiode," *Electronics Letters* **38**, pp. 327 – 328, Mar. 2002.
14. M. Inguscio, G. Moruzzi, K. M. Evenson, and D. A. Jennings, "A review of frequency measurements of optically pumped lasers from 0.1 to 8 THz," *Journal of Applied Physics* **60**, p. 161, Dec. 1986.
15. J. W. Brault, "High Precision Fourier Transform Spectrometry: The Critical Role of Phase Corrections," *Mikrochimica Acta* **3**, pp. 215–227, 1987.
16. M.-A. Parseval, "Mémoire sur les séries et sur l'intégration complète d'une équation aux differences partielle linéaires du second ordre, à coefficiens constans," *Académie des Sciences* , 1806. original submission was 5 April 1799.
17. M. Griffin, "Spire sensitivity models," Tech. Rep. Technical Report SPIRE-QMW-NOT-000642, Cardiff University, Cardiff, Wales, 2004.
18. M. Griffin, B. Swinyard, and L. Vigroux, "The herschel-spire instrument," in *Optical, Infrared and Millimeter Space Telescopes*, J. C. Mather, ed., **5487**, pp. 413–424, Proceedings of the International Society for Optical Engineering, 2004.